QUANTIFIYING THE EFFECT OF INTRAOCULAR PRESSURE ON THE ANTERIOR/POSTERIOR CORNEA VIA FD-OCT

An Honors Fellows Thesis

by

OSCAR CARRASCO-ZEVALLOS

Submitted to the Honors Programs Office
Texas A&M University
in partial fulfillment of the requirements for the designation as

HONORS UNDERGRADUATE RESEARCH FELLOW

April 2011

Major: Biomedical Engineering

QUANTIFIYING THE EFFECT OF INTRAOCULAR PRESSURE ON THE ANTERIOR/POSTERIOR CORNEA VIA FD-OCT

An Honors Fellows Thesis

by

OSCAR CARRASCO-ZEVALLOS

Submitted to the Honors Programs Office
Texas A&M University
in partial fulfillment of the requirements for the designation as

HONORS UNDERGRADUATE RESEARCH FELLOW

Approved by:

Research Advisor: Brian Applegate
Associate Director of the Honors Programs Office: Dave A. Louis

April 2011

Major: Biomedical Engineering

ABSTRACT

Quantifying the Effect of Intraocular Pressure on the Anterior/Posterior Cornea via FD-OCT. (April 2011)

Oscar Carrasco-Zevallos
Department of Biomedical Engineering
Texas A&M University

Research Advisor: Dr. Brian Applegate
Department of Biomedical Engineering

The presented research aims to develop an alternative and potentially superior method for diagnosing Glaucoma by relating IOP to deformation in different layers of corneal tissue via Fourier Domain Optical Coherence Tomography (FD-OCT), a non-invasive imaging technique. Glaucoma is a collection of disorders that results in damage to the optic nerve (cranial nerve II), which is responsible for relaying information from the retina to the brain. Although Glaucoma is incurable, surgery and medication can hinder its progression and prevent further damage to the optic nerve. Consequently, early detection of Glaucoma is imperative to minimize its noxious effects. Tonometry, a contemporary method used to test for Glaucoma, measures intraocular pressure (IOP) by relating the force of the tonometer to the resulting deformation of the ocular globe. However, data attained via tonometry is often unreliable due to the variations of ocular biomechanical properties from patient to patient. Using FD-OCT, depth profile images of rabbit cornea at different levels of intraocular pressure were attained *post mortem*.

The rabbit corneas were placed on an artificial anterior chamber; IOP was manipulated using water and a monometer. A correlation between fluctuations in the mechanical properties of the tissue and the differing levels of intraocular pressure was derived via different texture analysis methods, including the use of gray level co-occurrence matrices and different statistical calculations. Although the correlation attained was not robust, this study takes the first step to solidify a relationship between intraocular pressure and the mechanical properties of corneal tissue via FD-OCT.

ACKNOWLEDGMENTS

I would like to thank my research advisor, Dr. Applegate, for his patience and guidance throughout my project.

I would also like thank Janey, Nilanthi, and Sebina for their help throughout the past year.

Also, I would like to thank Ryan Shelton for his invaluable guidance, advice, and countless hours of conversation about research and life.

Lastly, I want to thank my family for their continuing support and encouragement.

NOMENCLATURE

FD-OCT	Fourier Domain Optical Coherence Tomography
FWHM	Full Width Half Max
GLCM	Gray Level Co-Occurrence Matrix
IOP	Intraocular Pressure
IR	Infrared
ND	Neutral Density

TABLE OF CONTENTS

Page

LIST OF FIGURES

LIST OF TABLES

CHAPTER I

INTRODUCTION

Glaucoma

Glaucoma is a collection of disorders that causes damage to the optic nerve (cranial nerve II) responsible for relaying information from the retina to the brain. Elevated levels of intraocular pressure (IOP) indicative of glaucoma are typically responsible for the injury resulting in permanent vision loss. Although Glaucoma is incurable, surgery and medication can hinder its progression and prevent further damage to the optic nerve. Consequently, early detection of Glaucoma is imperative to minimize its noxious effects.

Adult glaucoma is classified into two categories: open angle glaucoma and closed angle glaucoma. Open angle glaucoma, the more common of the two, occurs when the eye's drainage canals become obstructed over time. Aqueous humor, produced by the ciliary body within the eye, is unable to drain properly into the systemic circulation; consequently, the amount of fluid within the eye is increased resulting in elevated levels of IOP.

The blockage typically occurs at the trabecular meshwork—the tissue located at the base

---

This thesis follows the style of Optics Express.

of the cornea responsible for draining the aqueous humor into Schlemm's Canal. Fluid gradually collecting within the eye results in chronic vision loss. Medication and treatment at the early stages of vision loss can prevent further damage. Treatment includes beta blockers to reduce aqueous humor production and prostaglandin agonists to increase access to the drainage channels [1].

Closed angle glaucoma is caused by failure of the trabecular meshwork to drain fluid due to excessive contact between the meshwork and iris over time. Such prolonged contact induces the production of scar tissue that permanently blocks the drainage canals of the eye. Constant production of aqueous humor without appropriate drainage results in a rapidly elevated IOP and may produce symptoms such as vomiting, eye pain, and headaches [1]. However, closed angle glaucoma, also termed acute glaucoma, is usually asymptomatic until the onset of severe vision loss. The typical treatment for this disease is laser iridotomy, the surgical removal of tissue to prevent contact between the iris and trabecular meshwork.

Tonometry

Because ocular hypertension is a primary risk factor for glaucoma, IOP readings are often used for diagnosis. Tonometry measures IOP by relating the force of the tonometer to the resulting deformation of the ocular globe. Three main forms of tonometry are readily used by optometrists: indentation, applanation, and noncontact tonometers. Indentation tonometers physically displace a large intraocular area and

measure the IOP required to counterbalance the force of the tonometer. However, information attained from indentation tonometry is unreliable due to the unpredictable nature of the initial displacement and thus must be supported by empirical data to achieve satisfactory measurements [2]. In contrast, applanation tonometers induce constant deformations of the ocular globe, which enables scientists to directly calculate IOP. In addition, noncontact tonometers use a puff of air to indent a small section of the eyeball, and detectors measure the amount of time required for this deformation to return to its original configuration.

Several problematic assumptions result in inconsistent tonometry measurements. Tonometry was developed on the premise that all eyes respond similarly to an external force [3]. However, recent studies demonstrated that a variety of factors, including high myopia, vasoconstrictor therapy, and age-related macular degeneration, cause fluctuations in ocular rigidity [4]. Moreover, a steeper and/or thicker cornea causes a greater displacement of intraocular liquid during indentation tonometry Furthermore, LASIK, along with other surgical procedures can severely alter the biomechanical structure of the cornea. Consequently, these and other factors must be considered to accurately measure IOP.

Presented research

The presented research aimed to develop an alternative and potentially superior method for diagnosing Glaucoma by relating IOP to the biomechanical deformation of the

anterior/posterior cornea via Fourier Domain Optical Coherence Tomography (FD - OCT).

Relevant ocular anatomy

The sclera is a tough, protective layer composed of connective tissue that surrounds the eye. The cornea, a transparent disk of tissue, allows light to enter into the eye. Smooth muscles in the iris expand and contract to manipulate the size of the pupil, thus regulating the amount of light entering the eye. Situated behind the pupil, the lens focuses light onto the retina, a light-sensitive lining of the eye that contains photoreceptors. The chamber in front of the lens is filled with aqueous humor, a plasma-like fluid secreted by the ciliary epithelium [5]. In a healthy eye, drainage channels located on either side of the cornea allow the aqueous humor to enter the bloodstream. In glaucoma, these drainage channels become clogged, inducing a rise in IOP which damages the optic nerve.

Corneal structure

The cornea is composed of three distinct layers: the outer epithelium, the inner epithelium, and the central stroma. Supporting these layers are two specialized extracellular structures—the Bowman's and Descemet's membranes (Figure 1). The mechanical properties of these differ greatly; the epithelium layers are characterized by higher in-plane stiffness compared to the stroma, which constitutes 90% of corneal

thickness [6]. At the microscopic level, interlacing layers of collagen give rise to the mechanical properties of the stroma.

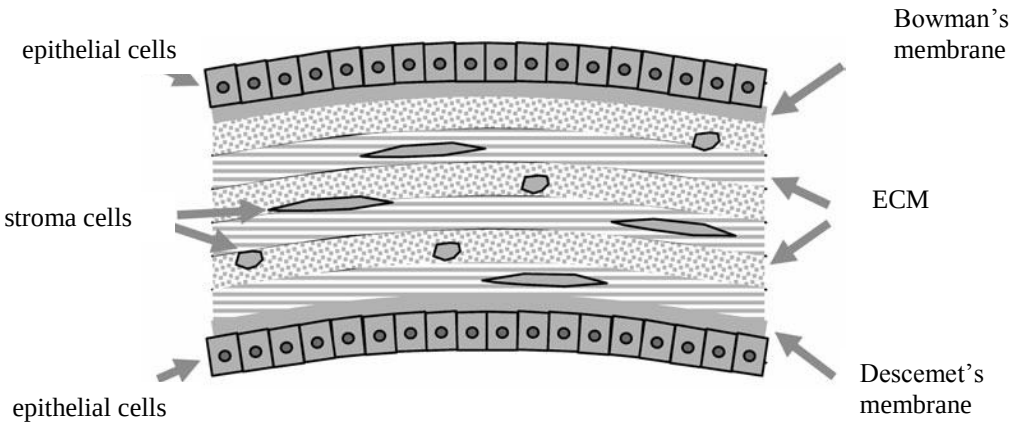

Figure 1. A depiction of the corneal structural makeup [6].

FD - optical coherence tomography

A typical OCT setup is depicted in Figure 2. A low-coherence source feeds light into a 2x2 coupler, which splits the intensity of the light into the reference arm and the sample arm. At the reference arm, a mirror, serving as a reference delay, is placed on a translation stage. Light exiting the sample arm is directed into a scanning mechanism, which scans the beam across the surface of the sample. Light backscattered from the sample mixes with light reflected from the reference arm resulting in interference at the spectrometer. The interference spectrum attained is processed into an A-line, the depth dependent reflectivity profile at a fixed lateral position on the sample. The beam is

scanned across the face of the sample, resulting in multiple A-scans that are complied into a two-dimensional cross-sectional image of the sample, i.e. a B-scan.

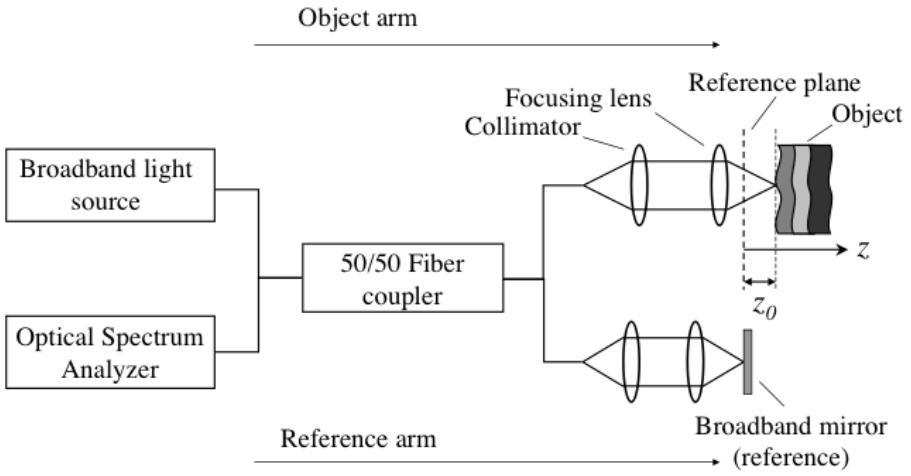

Figure 2. A typical optical coherence system [7].

There are two main types of FD-OCT: swept-source OCT and spectral domain OCT. The presented research employed spectral domain OCT to attain images of corneas. In this technique, a broadband light source is used to attain the whole spectral profile of the sample simultaneously. The interferometric signal is then analyzed in the Fourier-domain where a large DC term will be visible at the zero position, with artifacts appearing at negative and positive distances due to the Fast Fourier Transform performed on the raw data. The DC term can be easily subtracted by recording the amplitude of the spectral interferometric signal of the reference arm with the sample arm blocked and subtracting the resulting signal. The mirror artifacts can be accounted for by

ensuring that the reflective properties of the reference mirror will produce larger signals than the autocorrelation term [7].

Determination of relation between cornea deformation and IOP

Via non-linear microscopy, microstructural changes of the cornea were observed as IOP was increased [8]. More specifically, reduction in the size of collagen intra-lamellar gaps within the cornea was observed. The reduction in size of the intra-lamellar gaps was more prominent on the anterior cornea, rather than the posterior cornea where the pressure was applied. The hypothesis that drove the presented research was the following: we assumed that the alterations in the microstructure would affect the scattering properties of the cornea. Thus, such microstructural changes should be identifiable with FD-OCT, even though the intra-lamellar gaps are sub-resolution. Additionally, because the reduction in size is a function of depth, different layers of the stroma corresponding to different sizes of intra-lamellar gaps should be identifiable. As pressure is increased, such layers should become more pronounced, and their width would decrease in size. Such biometrics were analyzed to relate IOP to the biomechanical deformation of the cornea.

Previous studies

Recent studies attempted to characterize the biomechanical response of the cornea to intraocular pressure by employing numerical models. Some were able to replicate certain

mechanical properties of the human cornea under increased IOP via a hyperelastic, orthotropic material model [9]. Others have utilized structural engineering analysis tools, such mathematical shell analysis and non-linear finite element modeling, to investigate the mechanical behavior of the cornea under stress caused by disease [10]. Such models are currently being adapted to study keratoconus, a disease which causes degradation of corneal stroma.

Imaging techniques, such as X-ray scattering, were also used to map the organization of the collagen in the cornea and in the limbus, the tissue where the sclera and cornea meet [11]. The orientation of collagen around the limbus was found to be circumferential, while collagen in the central areas of the cornea is aligned in the nasal-temporal direction. Such information proved valuable in furthering our understanding of the mechanical responses of cornea to intraocular pressure.

Ophthalmology is one of the dominant fields of biomedical optics, including OCT imaging. This is mainly due to the high transmittance of the ocular media, enabling OCT to be used routinely to image posterior and anterior sections of the eye. Indeed, these images are useful in imaging and measuring the details of corneal pathologies [12]. Additionally, other novel methods, such as using ultra High-Resolution OCT imaging with a femtosecond laser light source to produce axial resolution of 1-3 μm are currently being developed to increase the prominence of OCT in a clinical setting [13].

Traditional biopsies introduce the risk of infection and spread of the disease. However, optical biopsies using OCT provide a noninvasive method of attaining the sufficient information to assess the tissue in question. Traditional OCT, with its high resolution, is capable of providing valuable information to the microstructure of tissue up to 1mm in depth[14]. Additionally, endoscopic intra-arterial OCT is another promising method in which thrombogenesis can be imaged and studied using a minimally-invasive technique [14].

Color Doppler imaging (CDI) is a method that is widely used to study how the hemodynamics of blood flow affects ocular diseases. CDI uses ultrasound waves to measure blood velocities in the ocular vasculature in relation to pressure. [15] Investigated how changes in intraocular pressure influence ocular blood flow and subsequently lead to a variety of retinal diseases such as diabetic retinopathy, retinal vein/artery occlusions, and ocular ischemic conditions.

Shear stress analysis is another common method used to study the role of blood flow and increased pressure in different retinal diseases. [16] showed that increased shear stress elevated the hydraulic conductivity of retinal endothelial cells. Furthermore, they tried to identify exactly which signaling pathways were responsible for the increased permeability of the blood-retinal layer. Although they concluded that Nitric Oxide played a crucial role in the process, [16] were not able to identify potential therapeutic targets.

Microaneurysms are often a product of a variety of ocular diseases including diabetic retinopathy. Identification of such structures can provide information about areas in the ocular vasculature at risk of rupture. [17] used a combination of indocyanine green angiography and High-Resolution OCT to identify microaneurysms with much success. Structures that were not possible to be identified with regular fluorescence angiography were easily detected with this new imaging technique.

CHAPTER II

METHODOLOGY

Fourier-domain optical coherence tomography

The source was a Super Luminescent Diode with a central wavelength of 830nm (Figure 3). The FWHM of the spectrum was close to 40 nm. The source transmitted the IR light into a 2x2 fiber coupler, where 50% of the intensity was emitted into each arm. The reference arm of the OCT system consisted of a collimator lens, a focusing lens with a focal length of 40 mm, and a mirror positioned on a translation stage to adjust the path length of the light. Additionally, a linearly variable ND filter was used to adjust the power of light in reference arm. The sample arm consisted of a collimating lens, which directed the light onto a galvo (Thorlabs) used to scan the beam across the surface of the sample. The galvo was controlled via LabVIEW and an analog output board (Measurement and Computing). A focusing lens with a focal length of 40 mm was used to focus onto the sample, which was placed in a x,y,z translator. The backscattered light traveled back through the 2x2 coupler and into a HR2000+ spectrometer (Ocean Optics).

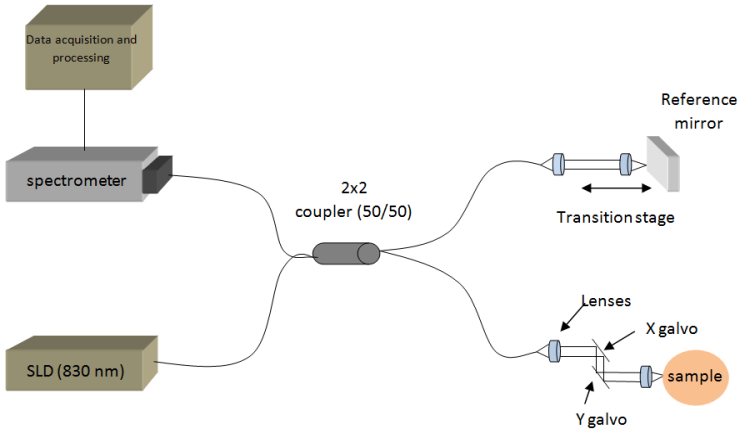

Figure 3. The basic setup of the FD-OCT system used.

The physics and principles of Optical Coherence Tomography are detailed in [7]; thus, only a brief overview will be presented here. The interference pattern resulting from the interference of light from both the sample arm and the reference arm was analyzed in the Fourier Domain. The DC signal, which emerged purely from the reference arm, was collected by blocking the sample arm and saving the resulting spectrum. The DC signal was then subtracted from the original signal, leaving only the cross-correlation terms intact to yield an A-line without the DC artifact. The A-lines represent the depth profile in the Fourier domain. B-scans, which are 2-D depth profile images comprised of a specified number of A-lines, were attained by scanning the beam across the surface of the sample. The calculated falloff of the system was close to 1 mm, while the experimental SNR was 102 dB for a perfect reflector, with an integration time of 50 microseconds and 2.5 mW incident on the sample. The theoretical shot-noise limited SNR was 108 dB. The calculated lateral resolution was 11 microns, assuming a

Gaussian beam shape. The raw spectra were collected in LabVIEW, and processed/displayed using Matlab.

Corneal analysis

Fresh rabbit corneas were obtained *post mortem*. The corneas were placed on an artificial anterior chamber and positioned at the focus of the sample arm in the OCT system. The intraocular pressure was manipulated using a syringe filled with water and a manometer. B-scans comprised of 600 A-lines were each attained at different intraocular pressures, namely at 5 mmHg, 10 mmHg, 15 mmHg, and 20 mmHg. A set of B-scans were compiled together to create volume scan.

Gray level co-occurrence matrix method

The initial texture analysis algorithm was based on the use of the gray level co-occurrence matrices (GLCM). Such a method has been proven useful in differentiating OCT images of different tissue samples based on their speckle patterns [18]. Speckle is typically produced via interference of wavefronts from a variety of scatterers within the focal volume of the OCT. It was assumed that the reduction in size of intra-lamellar gaps within the stroma as pressure is increased affects the speckle pattern of the image. Thus, by analyzing the speckle pattern of the attained FD-OCT images via the GLCM method, information about the intra-lamellar gaps could be attained indirectly.

GLCM is a spatial grey-level dependence method is based on the second-order joint conditional probability density function $f(i\ j|d, \theta)$. This function represents the probability that a pixel gray-level i is d pixels away at an angle θ from another gray-level pixel j [18]. If the image was restricted to N gray levels, the corresponding GLCM would be an NxN matrix (Figure 4). The GLCM was calculated via Matlab for each of the OCT images at the different pressures. The angle θ was restricted to 90˚ in order to attain features as a function of depth. The distance d was varied as a function of depth. Furthermore, the GLCM were restricted to 8 gray levels.

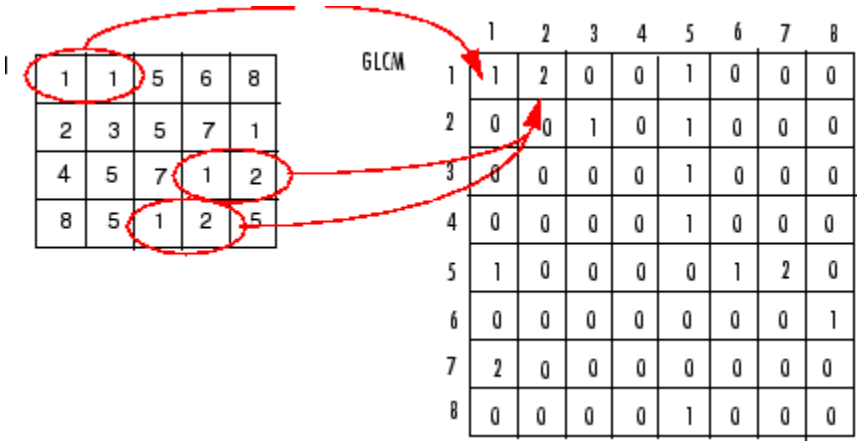

Figure 4: A typical example of a gray level co-occurrence matrix calculation. The 4x5 matrix represents the original pixel values of the image. Each element of the GLCM represents the probability density function as described above. In this example, the original image is restricted to 8 gray levels, thus yielding and 8x8 GLCM [18].

The features calculated included energy, homogeneity, and contrast defined in the following manner:

$$\text{Contrast} = \sum_{i.j} |i-j|^2 p(i.j) \quad (1)$$

$$\text{Energy} = \sum_{i.j} p(i.j)^2 \quad (2)$$

$$\text{Homogenetity} = \sum_{i.j} \frac{p(i.j)}{1+|i-j|} \quad (3)$$

Each of the calculated features corresponding to the different pressures was plotted as a function of depth. By inspection, the layers of the stroma were identified by analyzing the different minima and maxima of the curves, each corresponding to drastic changes in the calculated feature. A corneal stroma layer boundary was defined at the position in depth where a local maximum or minimum of the curve was located. Energy was the most frequently used feature for the analysis due to the well defined peaks at lower pressures. However, as the pressure was increased, the maxima and minima of the curves became less noticeable; consequently, the layers were less identifiable at high pressures.

An appropriate relation between IOP and the width of stromal layers was not able to be quantified using texture analysis based on GLCM's. Therefore, other texture analysis methods were employed as well.

Statistical method

Another texture analysis approach was used to solidify a relationship between IOP and

the microstructural changes in the cornea. As opposed to the previous method, which was primarily dependent on the visual characterization of stromal layers when analyzing the calculated features as a function of depth, the following approach was more mathematically based. The goal of the statistical method was to determine if certain calculated features could be used to statistically differentiate pre-defined layers in the cornea as a function of depth.

Using the data attained from the GLCM method, the OCT images at different pressures were segmented into 6 regions as a function of depth (this step will be clarified in the Results section). The boundaries of each region were chosen in accordance with results attained using the GLCM method (Figure 5). Furthermore, each of the six regions was subdivided into 20x20 pixel matrices. That is, region 1 was composed of 150 20x20 matrices, while region 2 was composed of 90 20x20 matrices and so on. Each of these 20x20 matrices served as single data points in the statistical analysis.

Laws' Filters were applied to each 20x20 matrix [19]. Laws Filters are a series of 5 filters that attempt to extract different texture components. More specifically, the filters are created as masks in Matlab and are designed to extract the following features in the image: level fluctuations, edges, gradients, waves, and ripples.

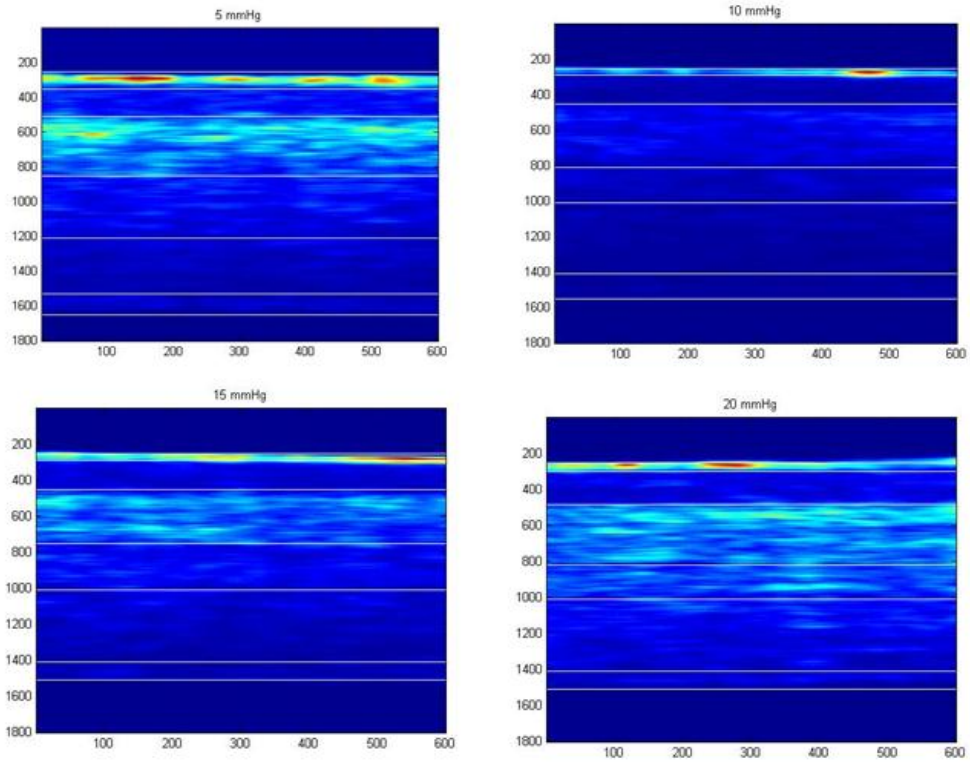

Figure 5: The segmented OCT images at different pressures. Each layer was divided into 20x20 matrices, which served as the data for the statistical analysis.

The masks used for the implementation of the filters were the following:

Level Filter= [1 4 6 4 1]

Edge Filter = [-2 -1 0 1 2]

Gradient Filter = [-1 0 2 0 -1]

Wave Filter = [-1 2 0 -2 1]

Ripple Filter = [1 -4 6 -4 1]

Each of the 5 filters was used in conjunction with each other; that is, the application of the Laws Filters [20] resulted in 25 filtered images for each 20x20 matrix. One filter was applied horizontally while the second filter was applied vertically across the image. For each of the filtered images for each 20x20 matrix, 5 features were calculated, namely mean, kurtosis, skewness, standard deviation, and energy. Therefore, for each 20x20 matrix, there were 125 calculations that were capable of describing a particular region.

The data for each 20x20 matrix were grouped together according to region. ANOVA was performed for the data sets corresponding to each region in order to determine if there was at least one region that was statistically different from the rest. Furthermore, t-tests comparing all the regions together were performed to identify which layers were statistically different. Confidence levels of 95% and 97.5% were used. In order to ensure that the different features could properly detect differently layers, another set of calculated data were collected using boundaries that were defined in close proximity to each other inside a region of the image expected to be homogeneous (Figure 6). Therefore, we expected that the t-tests for these newly defined boundaries would indicate that the regions were not statistically different. This served as a test to further ensure that the features could be used to correctly differentiate corneal stroma layers.

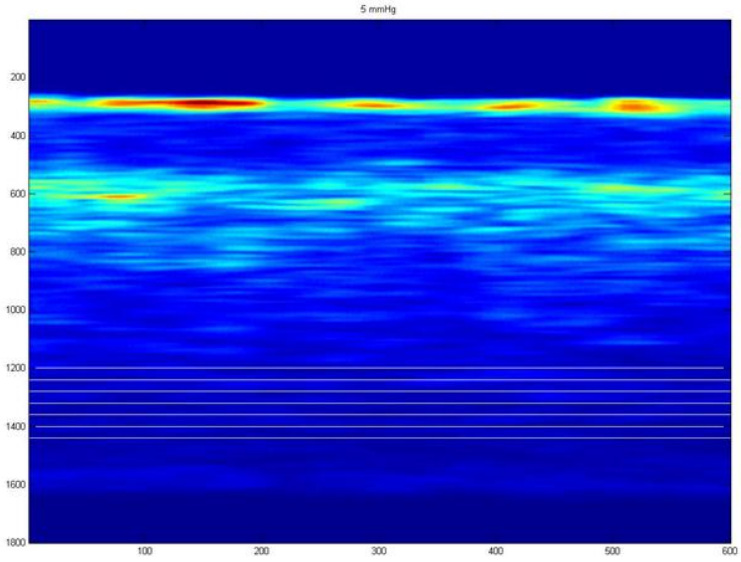

Figure 6: The corneal layers defined within a homogenous region. The region boundaries were chosen in such a way that the t-tests were expected to indicate that all the layers were statistically similar.

CHAPTER III

RESULTS

GLCM method

Using the standard texture analysis techniques available in Matlab—energy, contrast, and correlation calculations--the layers of the stroma at different intraocular pressures were able to be defined only at low pressures.

Volume OCT scans at different IOPs were compressed by averaging across the b-scans. The b-scans were plotted together to emphasize the effect of increasing the IOP, as seen in Figure 7.

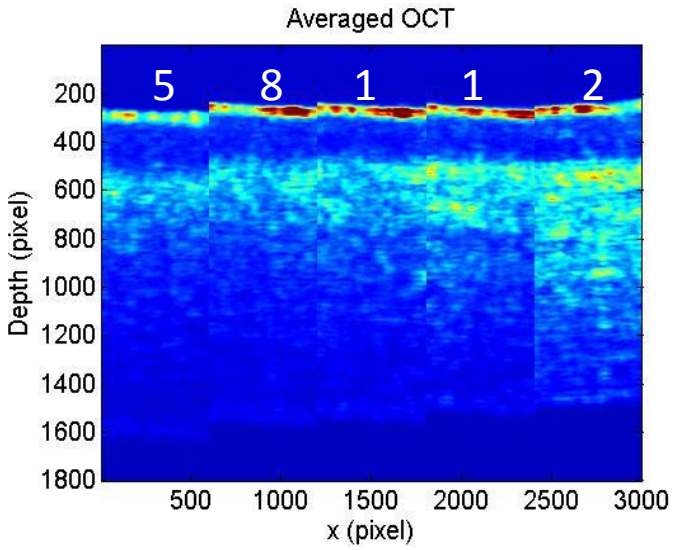

Figure 7: OCT images of cornea at different pressures. As evident, an increase in IOP yielded a decrease in the width of the cornea. Moreover, the contrast in anterior cornea tended to increase as the IOP pressure is increased.

As the IOP was increased, the contrast in the anterior cornea tended to increase. This change of contrast could be related to a change in the microstructure of the stroma. That is, as the pressure is increased, a resulting fluctuation in intra-lamellar gap size could yield a related change in the contrast of the image. In order to properly identify such a relation, the features calculated when using GLCM's were analyzed.

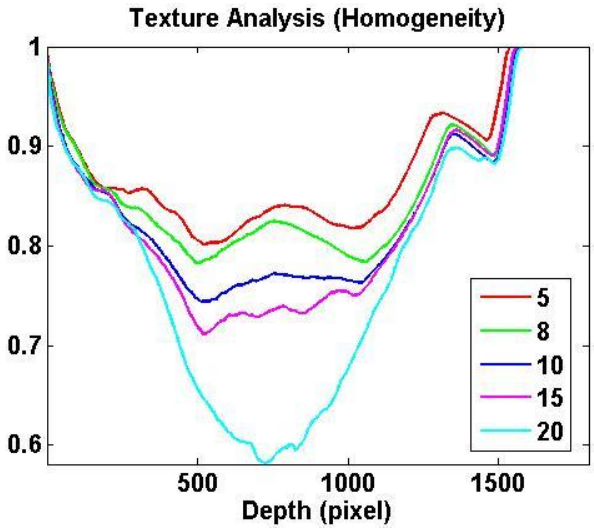

Figure 8: Homogeneity plotted as a function of depth. Any relation between homogeneity and increased IOP was difficult to discern due to the inconsistencies in the plots attained.

Homogeneity measures the closeness of pixel distribution values over a specified region. It appeared that around 750 pixels in depth, the homogeneity drops drastically as pressure was increased (Figure 8). Furthermore, the homogeneity at around 1350 pixels appears to be constant. However, there are not many features in the plots that are capable

of yielding useful information about layers in the cornea. As pressure is increased, the plots do not appear to show consistent features.

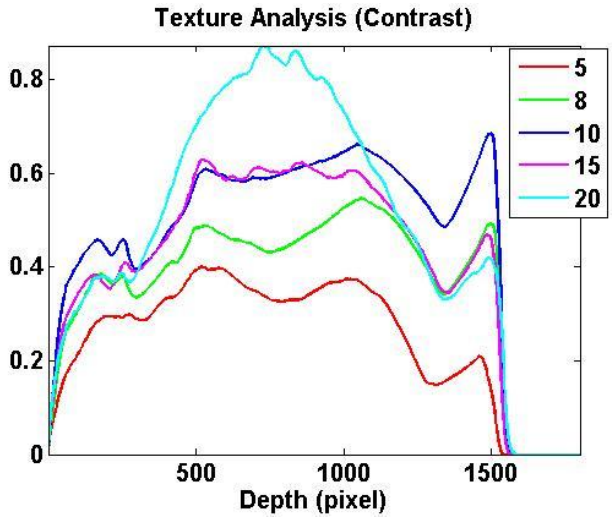

Figure 9: Contrast plotted as a function of depth. Due to the inconsistent data attained at different pressures, contrast was not able to be used to identify layers in the stroma.

Contrast measures how drastic the difference of pixel values is within a certain region. Similarly to homogeneity, contrast was a feature that could not be used to define layers in the stroma (Figure 9). Although some features in the curve tend to remain present as pressure is fluctuated, useful data could not be extracted using contrast due to the inconsistent maxima and minima in the curves. However, there appears to be a large increase in contrast around 500-1000 pixels as the pressure is increased to 20 mmHg.

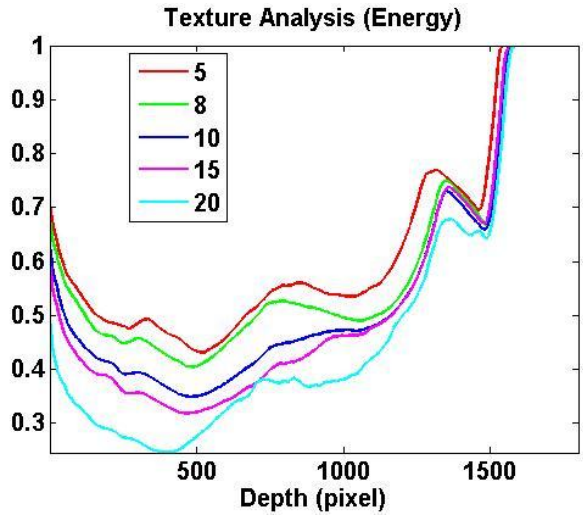

Figure 10: Energy plotted as a function of depth. At lower pressures, the energy curves appear to yield a consistent number of maxima and minima. However, at 20 mmHg, the different peaks were less identifiable, making it difficult to define where the layers of the corneal stroma were.

Overall, energy, defined as the sum squared elements in the gray-level co-occurrence matrix of the average OCT B-scan, was the most useful in determining the individual layers of the stroma. The different local maxima and minima of the curves were interpreted are radical changes in the energy of the area indicating a change in texture, which corresponded to a change in the microstructure of the cornea (see Figure 10). That is, the different layers were defined by unique texture properties that determined the energy within the region. However, as the pressure was increased, the different layers were less identifiable, as evident in Figure 11:

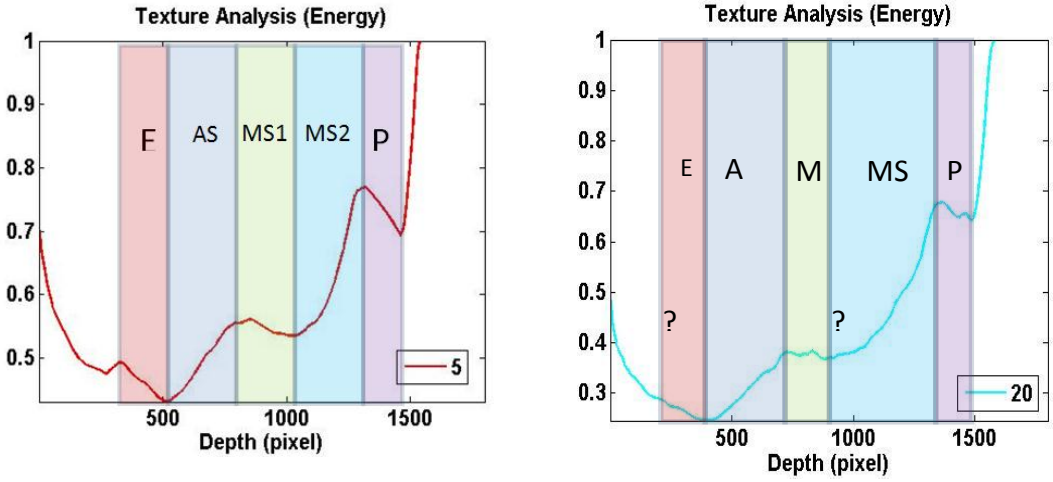

Figure 11: Using energy to define the corneal layers. The different layers of the stroma were attempted to be defined, where E is the epithelium, AS is the anterior stroma, MS1 is the first middle stroma layer, MS2 is the second middle stroma layer, and P is the posterior stroma.

Some of the maxima and minima evident at 5 mmHg of pressure disappeared when the cornea is subjected to a pressure of 20 mm Hg. Furthermore, some of the layers, including the anterior stroma and the middle stroma 2, tended to increase in length, which contradicted the initial assumption that all layers should compress under increased pressure. Moreover, results were not consistent when a new set of measurements were taken and the texture analysis process was repeated on the same cornea, as evident in Figure 12. The position of the layer boundaries, along with how many layers were able to be identified, was inconsistent.

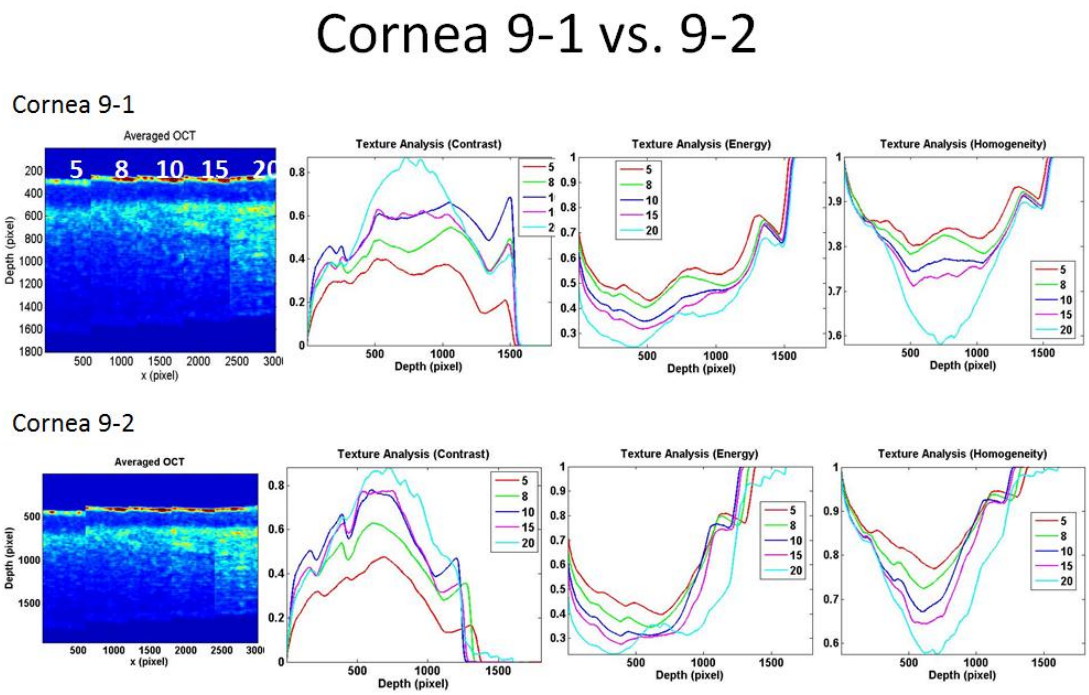

Figure 12: A comparison of the different features attained from different data sets for the same cornea. As evident, the same method of texture analysis yielded inconsistent results when applied to the different data sets from the same sample.

Overall, the GLCM method yielded inconsistent results not only when different pressures are applied, but also when different sets of data are taken from the same cornea as well. It can be concluded that while some of the calculated features may yield useful information, this texture analysis method cannot be used to derive a robust relationship between IOP and the biomechanical properties of the cornea.

Statistical method

The boundaries of the different layers in the stroma were estimated by analyzing the calculated energy as a function of depth (Figure 10). Using this information, the OCT

images were segmented and analyzed, as described in the Methodology section (Figure 6). The results of the ANOVA, more specifically the p values, are given in Table 1. A p value close to zero indicated that the null hypothesis could be rejected; that is, there was at least one data set (region) that was statistically different than the rest.

Table 1: ANOVA test results

	Energy	***Skewness***	***Kurtosis***	***Mean***	***Standard D.***
5 mmHg	0	0	0	0	0
10 mmHg	0	0	0	0	0
15 mmHg	0	0	0	0	0
20 mmHg	0	.0053	0	0	0

The results of the ANOVA test indicated that for the images at the four different pressures, there was at least one region which was statistically different than the rest for each feature. In order to determine which specific regions can be differentiated and which calculated features can best differentiate them, t-tests comparing the regions to each other were performed. Confidence levels of 95% and 97.5% were used. A value of 1 indicated that the two different regions were statistically different, while a value of 0 indicated otherwise. The results are given below in Tables 1-12:

Table 2: T-test results – Energy – α = .05

	1,2	*1,3*	*1,4*	*1,5*	*1,6*	*2,3*	*2,4*	*2,5*	*2,6*	*3,4*	*3,5*	*3,6*	*4,5*	*4,6*	*5,6*
5	1	1	1	1	1	1	1	1	1	1	1	1	1	1	1
10	1	1	1	1	1	1	1	1	1	1	1	1	1	1	1
15	1	1	1	1	1	1	1	1	1	1	1	1	1	1	1
20	1	1	1	1	1	1	1	1	1	1	1	1	1	1	1

Table 3: T-test results – Kurtosis – α = .05

	1,2	*1,3*	*1,4*	*1,5*	*1,6*	*2,3*	*2,4*	*2,5*	*2,6*	*3,4*	*3,5*	*3,6*	*4,5*	*4,6*	*5,6*
5	1	1	1	1	1	1	0	1	0	1	1	1	1	1	0
10	1	1	1	1	1	1	1	1	1	1	0	1	1	1	0
15	1	1	1	1	1	0	1	1	1	0	1	1	1	1	0
20	1	1	1	1	1	0	0	1	0	0	0	1	0	0	1

Table 4: T-test results – Mean – α = .05

	1,2	*1,3*	*1,4*	*1,5*	*1,6*	*2,3*	*2,4*	*2,5*	*2,6*	*3,4*	*3,5*	*3,6*	*4,5*	*4,6*	*5,6*
5	1	1	1	1	1	1	1	1	1	1	1	1	1	1	0
10	1	1	1	1	1	1	0	1	1	1	1	1	1	1	1
15	1	1	1	1	1	1	0	1	1	1	1	1	1	1	1
20	1	1	1	1	1	1	1	0	1	1	1	1	1	1	1

Table 5: T-test results – Skewness – α = .05

	1,2	*1,3*	*1,4*	*1,5*	*1,6*	*2,3*	*2,4*	*2,5*	*2,6*	*3,4*	*3,5*	*3,6*	*4,5*	*4,6*	*5,6*
5	**1**	**1**	**1**	**1**	**1**	**0**	**0**	**0**	**0**	**1**	**1**	**1**	**0**	**0**	**0**
10	**1**	**1**	**1**	**1**	**1**	**1**	**0**	**0**	**0**	**0**	**1**	**0**	**0**	**0**	**0**
15	**1**	**1**	**1**	**1**	**1**	**1**	**0**	**0**	**0**	**1**	**1**	**0**	**0**	**0**	**0**
20	**0**	**0**	**1**	**1**	**1**	**0**	**0**	**1**	**1**	**0**	**0**	**1**	**0**	**0**	**0**

Table 6: T-test results – Standard Dev. – α = .05

	1,2	*1,3*	*1,4*	*1,5*	*1,6*	*2,3*	*2,4*	*2,5*	*2,6*	*3,4*	*3,5*	*3,6*	*4,5*	*4,6*	*5,6*
5	**1**	**1**	**1**	**1**	**1**	**1**	**1**	**1**	**1**	**1**	**1**	**1**	**1**	**1**	**1**
10	**1**	**1**	**1**	**1**	**1**	**1**	**1**	**1**	**1**	**1**	**1**	**1**	**1**	**1**	**1**
15	**1**	**1**	**1**	**1**	**1**	**1**	**0**	**1**	**1**	**1**	**1**	**1**	**1**	**1**	**1**
20	**1**	**1**	**1**	**1**	**1**	**1**	**1**	**1**	**1**	**1**	**1**	**1**	**1**	**1**	**1**

Table 7: T-test results – Energy – α = .025

	1,2	*1,3*	*1,4*	*1,5*	*1,6*	*2,3*	*2,4*	*2,5*	*2,6*	*3,4*	*3,5*	*3,6*	*4,5*	*4,6*	*5,6*
5	**1**	**1**	**1**	**1**	**1**	**1**	**1**	**1**	**1**	**1**	**1**	**1**	**1**	**1**	**1**
10	**1**	**1**	**1**	**1**	**1**	**1**	**1**	**1**	**1**	**1**	**1**	**1**	**1**	**1**	**1**
15	**1**	**1**	**1**	**1**	**1**	**1**	**1**	**1**	**1**	**1**	**1**	**1**	**1**	**1**	**1**
20	**1**	**1**	**1**	**1**	**1**	**1**	**1**	**1**	**1**	**1**	**1**	**1**	**1**	**1**	**1**

Table 8: T-test results – Kurtosis – α = .025

	1,2	*1,3*	*1,4*	*1,5*	*1,6*	*2,3*	*2,4*	*2,5*	*2,6*	*3,4*	*3,5*	*3,6*	*4,5*	*4,6*	*5,6*
5	**1**	**1**	**1**	**1**	**1**	**0**	**0**	**1**	**0**	**1**	**1**	**1**	**1**	**0**	**0**
10	**1**	**1**	**1**	**1**	**1**	**1**	**1**	**1**	**1**	**0**	**1**	**1**	**0**	**0**	**0**
15	**1**	**1**	**1**	**1**	**1**	**0**	**1**	**1**	**1**	**0**	**1**	**1**	**1**	**0**	**0**
20	**1**	**1**	**1**	**1**	**1**	**0**	**0**	**1**	**0**	**0**	**0**	**1**	**0**	**0**	**1**

Table 9: T-test results – Mean – α = .025

	1,2	*1,3*	*1,4*	*1,5*	*1,6*	*2,3*	*2,4*	*2,5*	*2,6*	*3,4*	*3,5*	*3,6*	*4,5*	*4,6*	*5,6*
5	**1**	**1**	**1**	**1**	**1**	**1**	**1**	**1**	**1**	**1**	**1**	**1**	**1**	**1**	**0**
10	**1**	**1**	**1**	**1**	**1**	**1**	**0**	**1**	**1**	**1**	**1**	**1**	**1**	**1**	**1**
15	**1**	**1**	**1**	**1**	**1**	**1**	**0**	**1**	**1**	**1**	**1**	**1**	**1**	**1**	**1**
20	**1**	**1**	**1**	**1**	**1**	**1**	**1**	**0**	**1**	**1**	**1**	**1**	**1**	**1**	**1**

Table 10: T-test results – Skewness – α = .025

	1,2	*1,3*	*1,4*	*1,5*	*1,6*	*2,3*	*2,4*	*2,5*	*2,6*	*3,4*	*3,5*	*3,6*	*4,5*	*4,6*	*5,6*
5	**1**	**1**	**1**	**1**	**1**	**0**	**0**	**0**	**0**	**0**	**1**	**0**	**0**	**0**	**0**
10	**1**	**1**	**1**	**1**	**1**	**0**	**0**	**0**	**0**	**0**	**1**	**0**	**0**	**0**	**0**
15	**1**	**1**	**1**	**1**	**1**	**1**	**0**	**0**	**0**	**0**	**1**	**0**	**0**	**0**	**0**
20	**0**	**0**	**0**	**1**	**1**	**0**	**0**	**0**	**1**	**0**	**0**	**1**	**0**	**0**	**0**

Table 11: T-test results – Standard Dev. – α = .025

	1,2	***1,3***	***1,4***	***1,5***	***1,6***	***2,3***	***2,4***	***2,5***	***2,6***	***3,4***	***3,5***	***3,6***	***4,5***	***4,6***	***5,6***
5	**1**	**1**	**1**	**1**	**1**	**1**	**1**	**1**	**1**	**1**	**1**	**1**	**1**	**1**	**1**
10	**1**	**1**	**1**	**1**	**1**	**1**	**1**	**1**	**1**	**1**	**1**	**1**	**1**	**1**	**1**
15	**1**	**1**	**1**	**1**	**1**	**1**	**0**	**1**	**1**	**1**	**1**	**1**	**1**	**1**	**1**
20	**1**	**1**	**1**	**1**	**1**	**1**	**1**	**1**	**1**	**1**	**1**	**1**	**1**	**1**	**1**

The results of the t-tests using the close proximity boundaries as defined in the Methodology section (Figure 7) are given below in Table 12:

Table 12: T-test results – Cornea at 5 mmHg. – α = .025

	1,2	***1,3***	***1,4***	***1,5***	***1,6***	***2,3***	***2,4***	***2,5***	***2,6***	***3,4***	***3,5***	***3,6***	***4,5***	***4,6***	***5,6***
E	0	1	1	1	1	1	1	1	1	1	1	1	0	1	1
M	0	0	0	0	1	0	0	0	1	0	0	0	0	0	0
Skn	0	0	0	0	0	0	0	0	0	0	0	0	0	0	0
K	0	0	0	0	0	0	0	0	0	0	0	0	0	0	0
Std	0	1	1	1	1	1	1	1	1	1	1	1	0	1	1

where E = energy, M = mean, Skn = skewness, K = kurtosis, and Std = standard deviation.

CHAPTER IV

DISCUSSION

GLCM method

Through inspection, a variation in contrast in the averaged OCT images across different pressures could be noted. The contrast, which appeared to increase as function of depth as the pressure is increased, may signify a relation between pressure and the scattering of the OCT image—which was hypothesized depend on the microstructural properties of the cornea.

Using the GLCM method, the contrast, homogeneity, and energy were calculated for each of the averaged OCT images of cornea at different pressures. Overall, the plots of the different features as a function of depth did not provide much information about the microstructure of the stroma. That is, layers in the stroma, hypothesized to represent the differing sizes of intra-lamellar gaps as a function of depth, were not able to be clearly defined with varying IOP.

Contrast and homogeneity yielded inconsistent and sometimes erratic results as the IOP was increased. Furthermore, even at individual pressure levels, individual layers were undefinable. However, when energy was plotted as a function of depth, this feature appeared to reveal neatly defined layers at 5 mmHg. As previously mentioned, the maxima and minima of the energy curve, representing drastic changes in energy, were

interpreted as boundaries of the hypothesized stromal layers. As shown in Figure 11, five stromal layers were identified at 5 mmHg. However, as the pressure was increased to 20 mmHg, the maxima and minima of the curve became less clearly defined. Furthermore, some of the layers, including AS and MS2 appeared to increase in width, which contradicted the initial hypothesis that the stromal layers should compress as IOP is increased. It is possible that due to the lack of well-defined maxima and minima, the boundaries of the stromal layers at 20 mmHg were erroneously chosen.

When the GLCM method was applied to a different data set attained from the same cornea, the results obtained changed drastically. Some variation between data sets is expected; however, the inconsistencies presented in Figure 12 dictate that the GLCM method fails at attaining a robust relation between IOP and the microstructure of the cornea. The cause for such discrepancies in results for different data sets from the same sample may be due to the fact that while the GLCM method may be sufficient to differentiate between images of different types of homogenous tissues, it may not provide enough parameters to properly differentiate features within a non-homogenous image [18]. That is, the GLCM method may not be appropriate for image segmentation.

While the GLCM results indicated that a different texture analysis method must be used to appropriately relate IOP and the microstructure of the cornea, some interesting information was attained regarding the relationship between energy and the layers of the cornea. It appears that out of all the features calculated, energy as a function of depth

reveals clearly defined layers at 5 mmHg. Although these layers are less identifiable at higher pressures and somewhat inconsistent across different data sets, it can be concluded that of all the features calculated, energy appeared to have the strongest correlation to the microstructural properties of the cornea. Therefore, the layer boundaries defined at 5mmHg using Energy were the starting point for further analysis.

Statistical method

When analyzing the results from the multiple t-tests, it appeared that almost all of the features are capable of differentiating the pre-defined layers. However, the results from Table 12 indicated that energy and standard deviation appear to always differentiate layers even when the layers are defined in such a way that they are similar to each other. That is, the results given by energy and standard deviation may not be entirely reliable for defining layers. Therefore, Table 12 indicated that skewness, mean, and kurtosis were better suited to properly differentiate the different layers. The layers as defined by skewness (Table 5) across the different pressures are given below (Figure 13). Several of the original pre-defined six layers were deemed statistically similar to each other, and thus were grouped together. The boundaries of the new layers were defined when two consecutive predefined layers were statistically different. The results attained while using a confidence interval of 95% were used because they provided the most interpretable results. As evident, the number of layers across the different pressures was inconsistent. At 5 mmHg, there were 3 layers, while at 10 mmHg and 15 mmHg, there

were 4 layers. At 20 mmHg, the t-test results showed that there were not any boundaries as a function of depth.

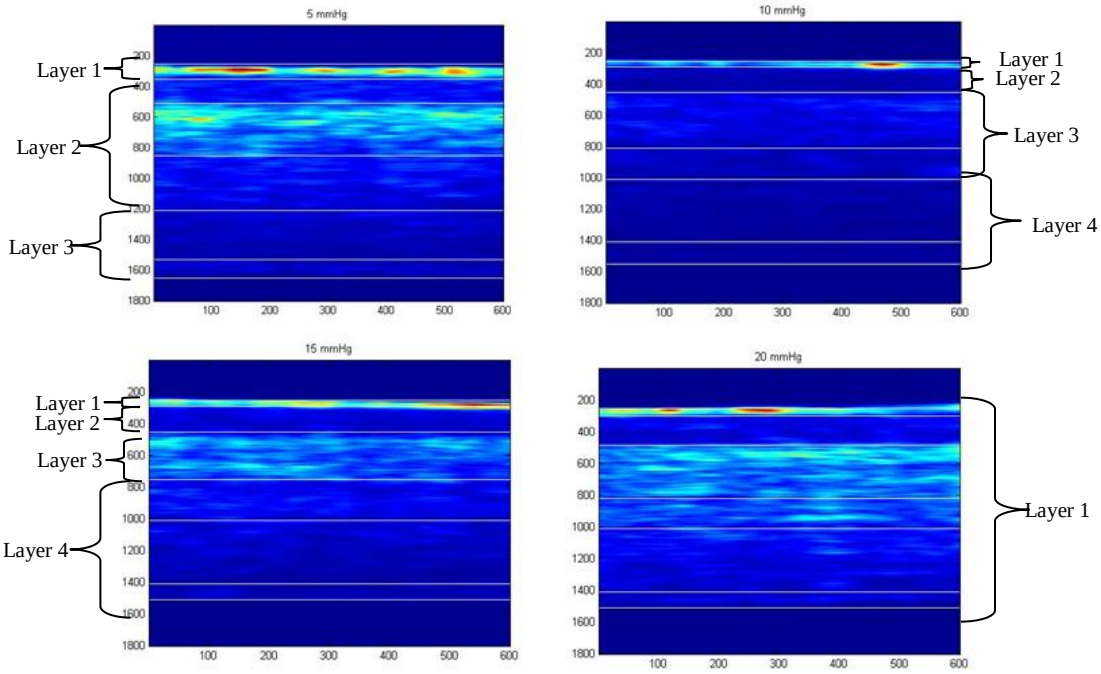

Figure 13: The stroma layers as defined by skewness. Across the different pressures, the layers were defined according to the results shown in Table 5. The number of layers seemed to be inconsistent across the different pressures. Furthermore, the results dictated that the 20 mmHg image contained only 1 layer.

Therefore, it can be concluded that skewness may not yield reliable results. That is, the number of layers defined by the data is too inconsistent across the different pressures.

The results attained for kurtosis are shown on Table 3. As before, some of the predefined layers were determined to be statistically similar and were grouped together. Moreover, the boundaries of the new layers were defined at points at which the t-tests determined

that two consequently layers were statistically different. The layers as defined by kurtosis are given below (Figure 14).

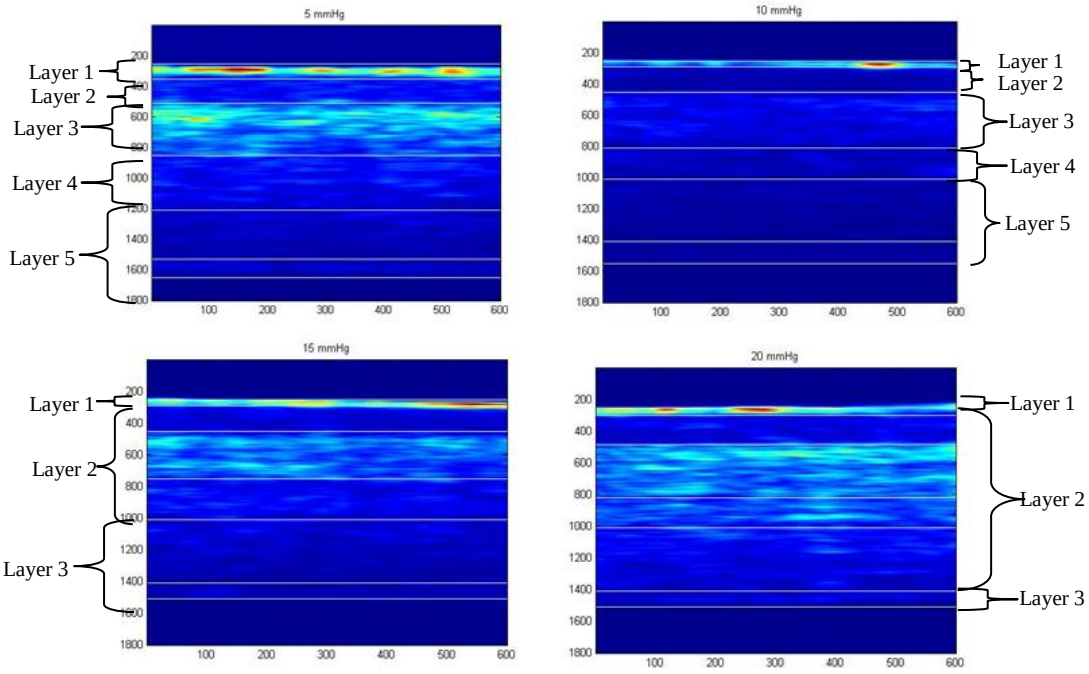

Figure 14: The stroma layers as defined by kurtosis. Across the different pressures, the layers were defined according to the results shown in Table 3. The number of layers seemed more consistent across different pressures than when using Skewness. However, it also appeared that the number of layers decrease as the pressure increases.

The layers as defined by the data given in Table 3 indicated that the number of layers decreased as the pressure was increased. At pressures 5 mmHg and 10 mmHg, there were five distinguishable layers. However, at 15 mmHg and 20 mmHg, there appeared to be only three layers. The reason for this may be that as pressure is increased, the microstructure in the anterior and posterior cornea differs more than the microstructure in the middle stroma. The microstructure might become more homogenous in the center

of the cornea. Furthermore, the outer layers seem to shrink while the inner layer appears to grow wider, which is a phenomenon that was also noted when using the GLCM method. Lastly, out of the five calculated features, kurtosis was able to best differentiate a consistent number of layers across the four different pressures. While skewness was able to properly differentiate layers at certain pressures, the number of layers defined was not consistent as pressure was increased. All other features were not able to properly differentiate the corneal stroma layers.

CHAPTER V

CONCLUSION

While there were certain features in each method that yielded some desirable results, a concrete definition of layers based on the microstructure of the corneal stroma was unable to be determined. Furthermore, a substantial correlation between pressure and the number of layers could not be derived. However, the experiments and methods attempted here constitute the first and necessary step towards developing a novel method to diagnose Glaucoma via FD-OCT. Certain features, such as energy when using the GLCM method, and kurtosis when using the statistical method, yielded positive results and could provide a starting point for future analysis. Furthermore, other texture analysis methods and tools, such as Gabor filtering and 2-D Fast Fourier Transforms could be used in future studies to solidify a relationship between the microstructure of the corneal stroma and IOP via FD-OCT.

REFERENCES

[1] Glaucoma Research Foundation, "Glaucoma." www.Glaucoma.org, accessed on 4/1/11.

[2] M. B. Shields, *The Textbook of Glaucoma* (Williams & Wilkins, Media, Pennsylvania 1998).

[3] D. F. Garway-Heath, "The effect of corneal biomechanics on tonometry." Review of Optometry **142,** 8-9 (2005).

[4] J. Liu and C. Roberts, "Influence of corneal biomechanical properties on intraocular pressure measurement: Quantitative analysis." Journal of Cataract & Refractive Surgery **31,** 146-155 (2005).

[5] R. P. Crick, *A Textbook of Clinical Ophthalmology: A Practical Guide to Disorders of the Eyes and Their Management* (World Scientific, London 2003).

[6] K. Anderson, A. El-Sheikh, and T. Newson, " Application of structural analysis to the mechanical behaviour of the cornea," Journal of the Royal Society **5**, *2*,3-15 (2004).

[7] J. Izatt A. and M. Choma A., "Theory of optical coherence tomography," in *Optical Coherence Tomograpy - Technology and Applications*, G. James Fujimoto and D. Wolfgang, eds, pp. 47 (Springer, New York, 2008)

[8] Q. Wu, B.E. Applegate, and A. T. Yeh,"Cornea microstructural and mechanical response measured using optical coherence and nonlinear optical microscopy with sub-10-fs pulses," Frontiers in Optics, Optical Society of America, San Jose, CA, October, 2009

[9] A. Pandolfi and F. Manganiello, "A model for the human cornea: constitutive behavior and numerical Analysis," Biomechanics and Modeling in Mechanobiology **5,** 237-246 (2006).

[10] H. Studer, X. Larrea, and H. Riedwyl, " Biomechanical model of human cornea based on stroma microstructure," Journal of Biomechanics **43,** 836-842 (2010).

[11] H. Aghamohammadzadeh, R. Newton, and K. Meek, " X-Ray scattering used to map the preferred collagen orientation in the human cornea and limbus," Structure **12,** 249-256 (2004).

[12] J. Jasapara C., S. Wielandy, and A. Yablon D., "Fourier domain optical coherence tomography – a new platform for measurement of standard and microstructured fibre dimensions," IEE Proc. Optoelectron. **153,** 229-234 (2006).

[13] W. Drexler, T.H, Ko, H. Sattmann, B. Hermann, M. Stur, et al, "Clinical feasibility of ultrahigh resolution ophthalmic optical coherence tomography," Investigative Opthalmology and Visual Science **43,** 264-273, (2002).

[14] A. Fercher F., W. Drexler, C. Hitzenberger K., and T. Lasser, " Optical coherence tomography - principles and applications," Rep. Prog. Phys. **66,** 239-245 (2003).

[15] G. Dimitrova and S. Kato, "Color doppler imaging of retinal diseases," Survey of Opthalmology **55,** 193-214 (2010).

[16] Lakshminarayanan, T. Gardner W., and Tarbell,John,M., "Effect of shear stress on the hydraulic conductivity of cultured bovine retinal microvascular endothelial cell monolayers," Current Eye Research, **21,** 944 -951(2000).

[17] A. Bourhis, J. Girmens, S. Boni, F. Pecha, C. Favard, J. Sahel, and M. Paques, "Imaging of macroaneurysms occurring during retinal vein occlusion and diabetic retinopathy by indocyanine green angiography and high resolution optical coherence tomography," Graefes Arch Clin Exp Ophthalmol **248,** 161-166, (2010).

[18] W. Gossage, T. S. Tkascyzk, J. J. Rodriguez, and J. K. Barton, "Texture analysis of optical coherence tomography images: feasibility for tissue classification," Journal of Biomedical Optics **8,** 570-575 (2003).

[19] Pfisterer, Richard, and Farzin Aghdasi. "Detection of Masses in Digitised Mammograms." Proceedings of the 1998 South African Symposium on Communications and Signal Processing , Rondebosch, South Africa, 115-20 (1998)

CONTACT INFORMATION

Name:	Oscar Carrasco-Zevallos
Professional Address:	c/o Dr. Brian Applegate Department of Biomedical Engineering 335s Zachary Engineering Center 3120 TAMU College Station, TX 77843
Email Address:	moz0817@gmail.com
Education:	B.S., Biomed. Eng., Texas A&M University, May 2012 Summa Cum Laude Honors Research Fellow Alpha Eta Mu Beta